Large Scale Structure and Kinematics of the Dwarf Irregular Galaxy HoII

M. Bureau[1] and C. Carignan[2]

[1]Mount Stromlo and Siding Spring Observatories
The Australian National University, Australia
martin@mso.anu.edu.au

[2]Département de Physique and Observatoire
Astronomique du Mont Mégantic
Université de Montréal, Canada
claude@astro.umontreal.ca

Abstract: We present VLA D-array HI observations of the M 81 group dwarf irregular galaxy HoII. We detect a previously unknown extended but low surface brightness component N-W of the galaxy, probably caused by ram pressure from the intergalactic medium. The fairly regular velocity field allows us to extend the kinematical information to large radii. It is shown that pressure support is important in HoII and a rotation curve corrected for asymmetric drift is derived. However, due to unreliable optical photometry, a mass model of the galaxy is not available yet, and new observations are necessary before the dark matter content of HoII can be constrained.

Introduction

The goal of this project is to extend the range of well-studied galaxies to the extreme faint end of the galaxy luminosity and mass distributions, and to study environmental effects on such systems.

The dwarf irregular galaxy HoII offers such an opportunity. It is a member of the close-by M 81 group (D=3.2 Mpc), possesses a faint envelope, a bright compact blue core with intense star formation, and an extended gas disk.

Puche et al. (1992) obtained multi-configurations VLA HI observations HoII. Their study concentrated on the small to medium scale structure of the ISM, shells in particular, and its relationship to star formation.

In this study, we are interested in the large scale structure and kinematics of the gas, with the goal of constructing a complete mass model for HoII, and constraining the dark matter distribution.

We used the D-array data of Puche et al. (1992) to construct a low-resolution naturally weighted HI cube of HoII (67″ circular Gaussian beam). This data cube forms the basic dataset on which our analysis is based. Its global properties are summarized in Table 1 below.

F_{HI} (Jy km s^{-1})	M_{HI} ($M_\odot$)	V_{sys} (km s^{-1})	ΔV_{20} (km s^{-1})	ΔV_{50} (km s^{-1})
267.1	6.44×10^9	156	72	57

Table 1: HoII global HI properties

HI Distribution

Channel Maps:

The channel maps for the naturally weighted cleaned cube are shown in Figure 1. Important points to note are:

- Many large HI shells and holes are visible.
- A rotation pattern, although weak, is present on both side of the galaxy, especially at the extreme velocity channels.
- The position angle changes with distance from the galaxy center, indicating the presence of a warp in the HI disk.
- The S-W cloud is easily detected, and extends the information up to a radius of $15'$ in that direction ($4\ R_{25}$).
- The HI is more extended than previous observations led us to expect. On the northern side, HI is observed up to $15'$ again.

Total HI Map:

The integrated HI distribution (MOM0) is shown in Figure 2. Additional points to note are:

- Although the HI emission increases smoothly in the inner regions, the shells and holes perturb the distribution significantly.
- The S-W cloud and the northern structure seem to merge and form a very extended but low surface brightness component extending over the entire N-W half of the galaxy. This faint structure is detected for the first time and covers an area equivalent to the brighter, previously known portions of the galaxy.
- There is a strong asymmetry in the HI distribution (with respect to a NE-SW axis) and a steep ridge on the S-E side. The structure seen indicates that HoII is probably affected by ram pressure, presumably from the intergalactic medium of the M81 group.

H I Kinematics

Velocity Field:

The faint N-W component in HoII is important, allowing to extend the kinematical information (e.g. the rotation curve) by a factor of 2 compared to previous studies, such as that of Puche et al. (1992).

The H I velocity field (MOM1) is shown in Figure 3. Important points to note are:

- The rotation pattern is clearly visible on both side of the galaxy.
- A significant warp is present in the outer regions of the disk, as seen from the change in position angle outside $R \approx 4'$.
- The isovelocity contours close at $R \approx 7'$, indicating that the rotation curve should reach its maximum around that radius.
- Although the velocities in the N-W component are similar to those of neighbouring regions, the rotation pattern is significantly disturbed. A non-rotational component seems to dominate the kinematics in the outer parts, and it is not clear that the H I is in dynamical equilibrium.

Velocity Dispersion Field:

The H I velocity dispersion field (MOM2) is shown in Figure 4. Important points to note are:

- The presence of shells and holes is obvious in the center of the galaxy.
- The velocity dispersion increases gradually from the outer parts to the inner parts, where it reaches values of $\approx 16 - 17$ km s^{-1}.
- The velocity dispersion in the N-W component is low (≤ 7 km s^{-1}) and fairly homogeneous.

Rotation Curve

Uncorrected Rotation Curve:

The HI velocity field was modeled using the now standard tilted ring algorithm ROTCUR (Begeman 1989). HoII center and systemic velocity were first solved for and then kept fixed while solving for the inclination, position angle, and rotation velocity of each ring. The complete rotation curve is shown in Figure 5 below, although the solution for $R \geq 700''$ is not so well defined.

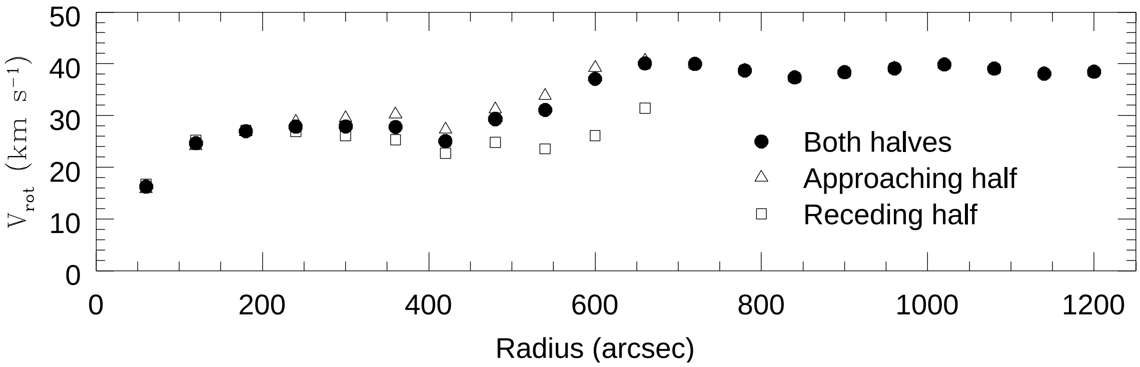

Figure 5: HoII uncorrected rotation curve.

The two important points to note are:

- After a rapid rise, the rotation curve flattens around 27 km s^{-1} until $R \approx 400''$, and then increases again to $\approx$ 39 km s^{-1} until the last measured point. Because the optical radial extent of the galaxy is only $4'$ (at R_{25}), HoII must contain significant amount of dark matter in the outer parts.
- The rotation velocity in the inner parts is only $\approx$ 27 km s^{-1}, while the velocity dispersion is $8 - 15$ km s^{-1} in those regions. Pressure support must therefore be non-negligible in the inner parts.

Asymmetric Drift Correction:
The ratio σ_V^2/V_{rot}^2 is typically 0.15-0.25 in the inner parts, suggesting that in addition to rotation, random motions may provide significant dynamical support. This effect can be treated as a correction σ_D to apply to the observed rotation velocity V_{rot}, in order to get the true circular velocity V_c required to balance the galaxy's gravity by pure rotation. Following Meurer et al. (1996), we have:

$$V_c^2 = V_{rot}^2 + \sigma_D^2, \quad \text{where:} \qquad \sigma_D^2 \simeq -R\sigma_V^2 \; \frac{\partial \ln(\Sigma_{HI}\sigma_V^2)}{\partial R}$$

Using the tilted ring model, radial profiles for σ_V and Σ_{HI} can be obtained and the asymmetric drift correction calculated. The corrected rotation curve (circular velocity curve) is shown in Figure 6 below.

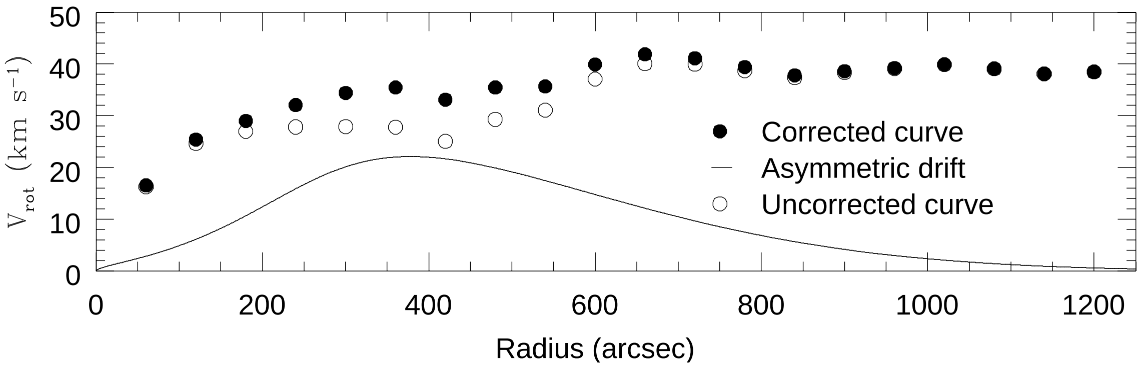

Figure 6: HoII corrected rotation curve.

The two important points to note are:

- Pressure support is significant for $200'' \leq R \leq 600''$.
- The rotation curve is better behaved and now reaches 34 km s^{-1} in the inner regions, while remaining flat at 39 km s^{-1} up to $R = 1200''$. This strengthens the case for dark matter, and indicates that it must dominate HoII mass distribution at almost all radii.

Conclusion & Future Work

Using low resolution HI synthesis observations, we have detected an extended but faint structure N-W of the dwarf galaxy HoII, probably caused by ram pressure from the intergalactic medium in the M 81 group.

This component allowed us to extend the kinematical information by a factor of 2 in distance compared to previous studies, but also raised doubt that the gas is in dynamical equilibrium in the outer parts.

Nevertheless, a rotation curve corrected for pressure support was derived, and it remains flat until the last measured point at $R = 1200''$, implying that HoII is dark matter dominated at almost all radii.

We have obtained R-band images of HoII but the photometry has proven unreliable. This has prevented us from constructing a complete mass model of HoII (stars + gas + dark matter), but the dark matter distribution will be constrained once better photometry is obtained.

The possible effects of ram pressure on the structure, kinematics and star formation history of HoII will also be investigated in more details in the future.

Acknowledgements

We wish to thank D. Puche & K. C. Freeman for useful discussions. M. Bureau acknowledges the support of an Australian DEETYA Overseas Postgraduate Research Scholarship, a Canadian NSERC Postgraduate Scholarship, and an Astronomical Society of Australia travel grant to attend this meeting.

The Digitized Sky Surveys were produced at the Space Telescope Science Institute under U.S. Government grant NAG W-2166. The images of these surveys are based on photographic data obtained using the Oschin Schmidt Telescope on Palomar Mountain and the UK Schmidt Telescope.

References

Begeman, K. G. 1989, A&A, 223, 47
Meurer, G. R., Carignan, C., Beaulieu, S. F., & Freeman, K. C. 1996, AJ, 111, 1551
Puche, D., Westpfahl, D., Brinks, E., & Roy, J.-R. 1992, AJ, 103, 1841

Figure 1: HoII HI line channel maps. The heliocentric velocities are displayed in the top right corner of each channel. The $67'' \times 67''$ beam is shown in the bottom left corner of the first channel on each page. Contours are 1, 3.5, 7, 14, 21, and 28 K.

Figure 2: HoII total HI map, superposed on a gray scale Digitized Sky Survey image. Contours are 1, 3, 6, 10, 20, 40, 60, 90, 120, 150, and 180 $\times$ 1E19 atoms cm^{-2}.

Figure 3: HoII HI velocity field, superposed on a gray scale Digitized Sky Survey image. Contours are 120, 130, 135, 140, 150, 160, 170, 175, and 180 km s^{-1}. The plot on the next page shows a color version of the velocity field only.

Figure 4: HoII HI velocity dispersion field, superposed on a gray scale Digitized Sky Survey image. Contours are 6, 9, 12, 15, 18, and 21 km s^{-1}. The plot on the next page shows a color version of the velocity dispersion field only.

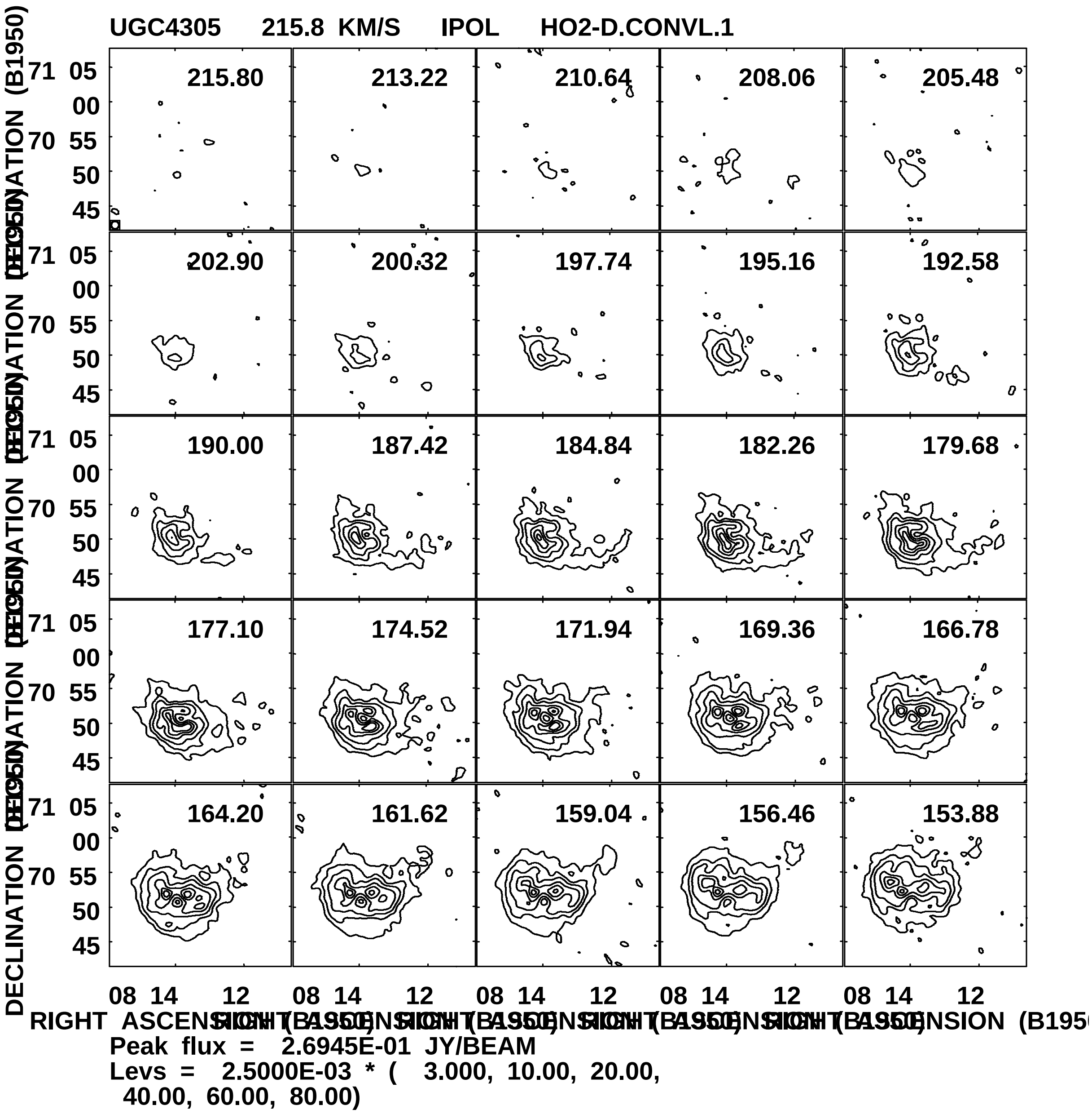
UGC4305 215.8 KM/S IPOL HO2-D.CONVL.1
215.80
213.22
210.64
208.06
205.48
202.90
200.32
197.74
195.16
192.58
190.00
187.42
184.84
182.26
179.68
177.10
174.52
171.94
169.36
166.78
164.20
161.62
159.04
156.46
153.88
DECLINATION (B1950)
71 05
00
70 55
50
45
08 14
12
RIGHT ASCENSION (B1950)
Peak flux = 2.6945E-01 JY/BEAM
Levs = 2.5000E-03 * (3.000, 10.00, 20.00, 40.00, 60.00, 80.00)

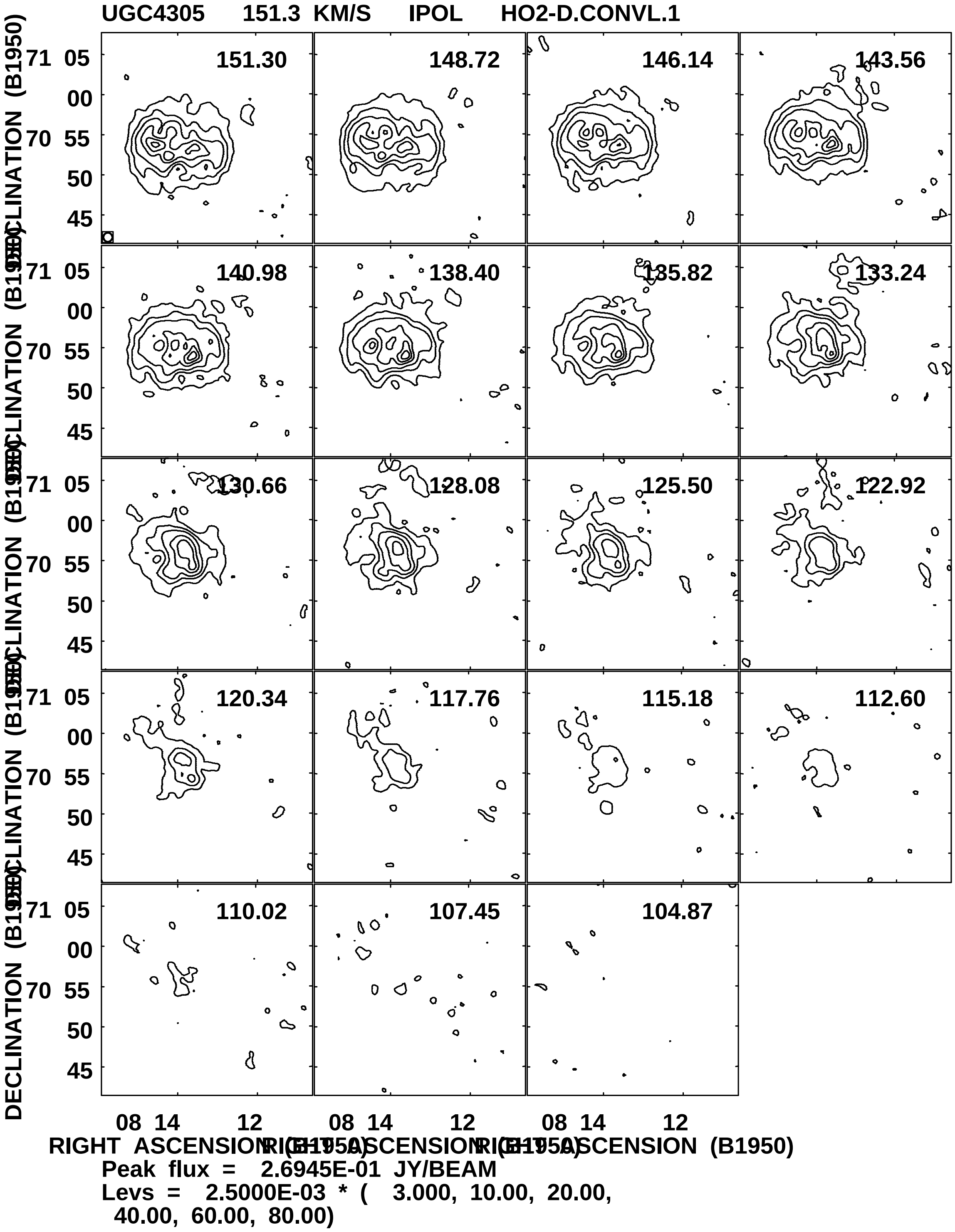

UGC4305 151.3 KM/S IPOL HO2-D.CONVL.1
151.30
148.72
146.14
143.56
140.98
138.40
135.82
133.24
130.66
128.08
125.50
122.92
120.34
117.76
115.18
112.60
110.02
107.45
104.87
DECLINATION (B1950)
71 05
00
70 55
50
45
RIGHT ASCENSION (B1950)
08 14
12
Peak flux = 2.6945E-01 JY/BEAM
Levs = 2.5000E-03 * (3.000, 10.00, 20.00,
40.00, 60.00, 80.00)

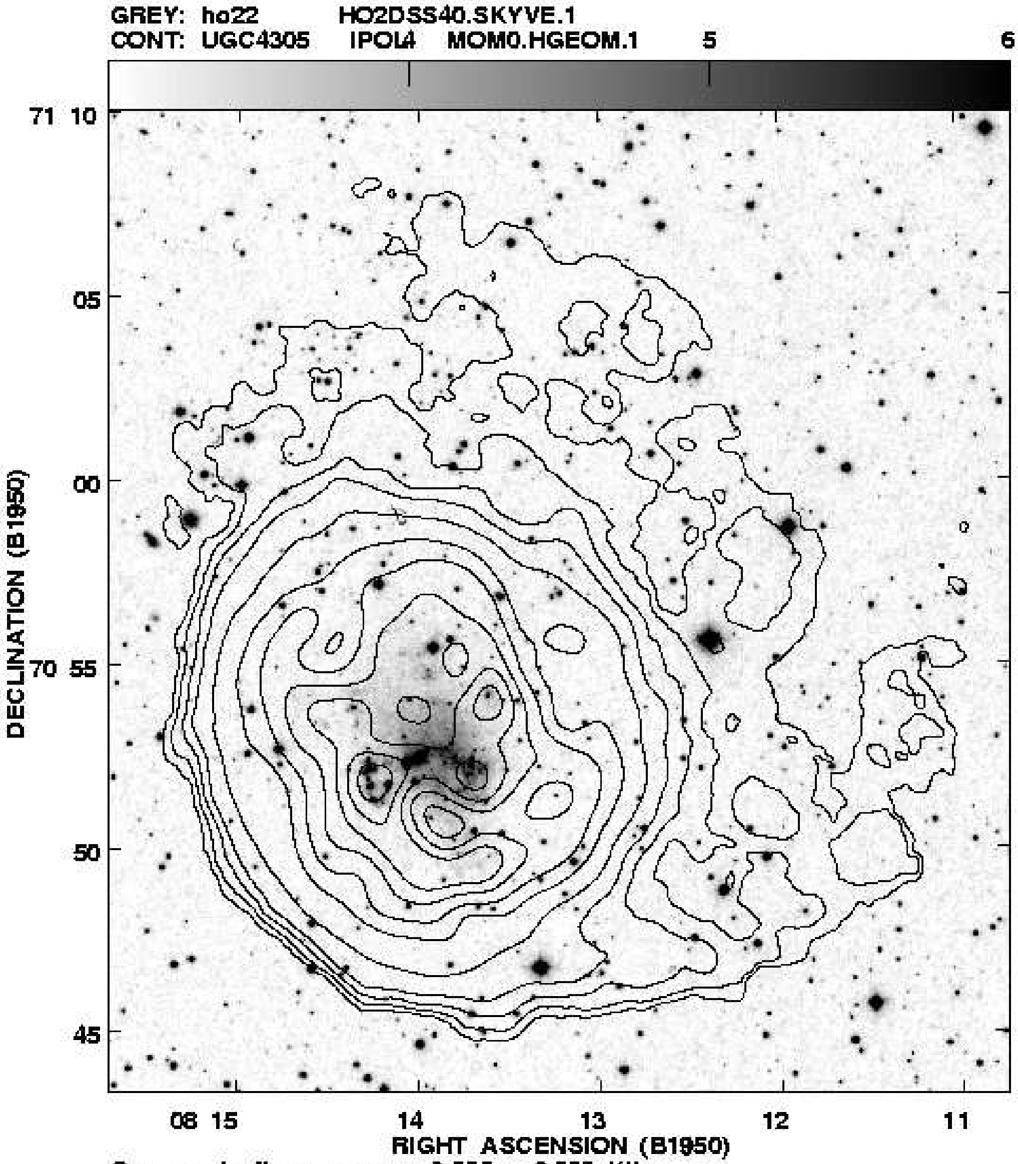

Grey scale flux range= 3.000 6.000 Kilo
Peak contour flux = 8.4914E+03 JY/B*M/S
Levs = 8.4285E+01 * (0.500, 1.500, 3.000, 5.000, 10.00, 20.00, 30.00, 45.00, 60.00, 75.00, 90.00)

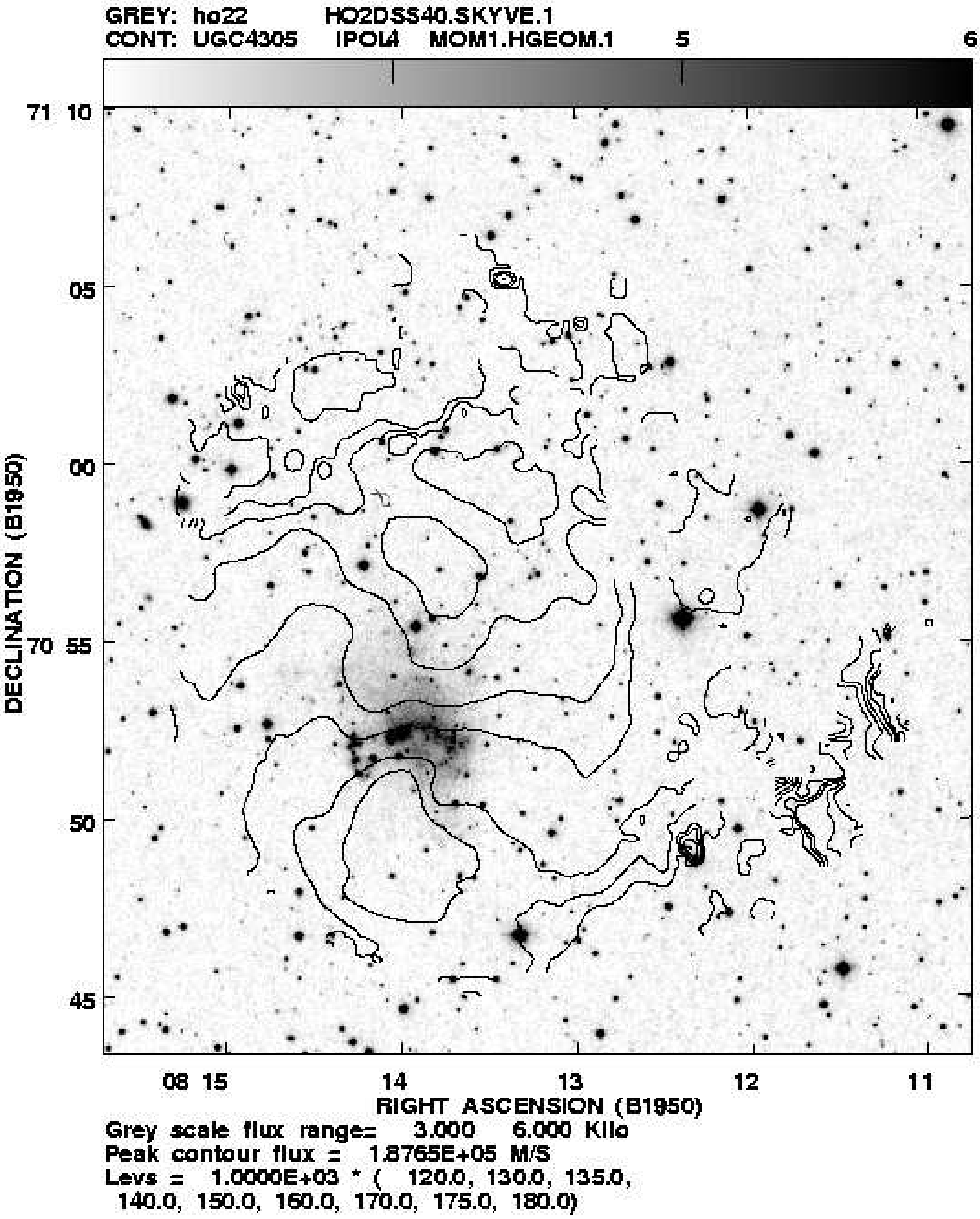
GREY: ho22 HO2DSS40.SKYVE.1
CONT: UGC4305 IPOL4 MOM1.HGEOM.1
5
6
71 10
05
00
70 55
50
45
DECLINATION (B1950)
08 15
14
13
12
11
RIGHT ASCENSION (B1950)
Grey scale flux range= 3.000 6.000 Kilo
Peak contour flux = 1.8765E+05 M/S
Levs = 1.0000E+03 * (120.0, 130.0, 135.0,
140.0, 150.0, 160.0, 170.0, 175.0, 180.0)

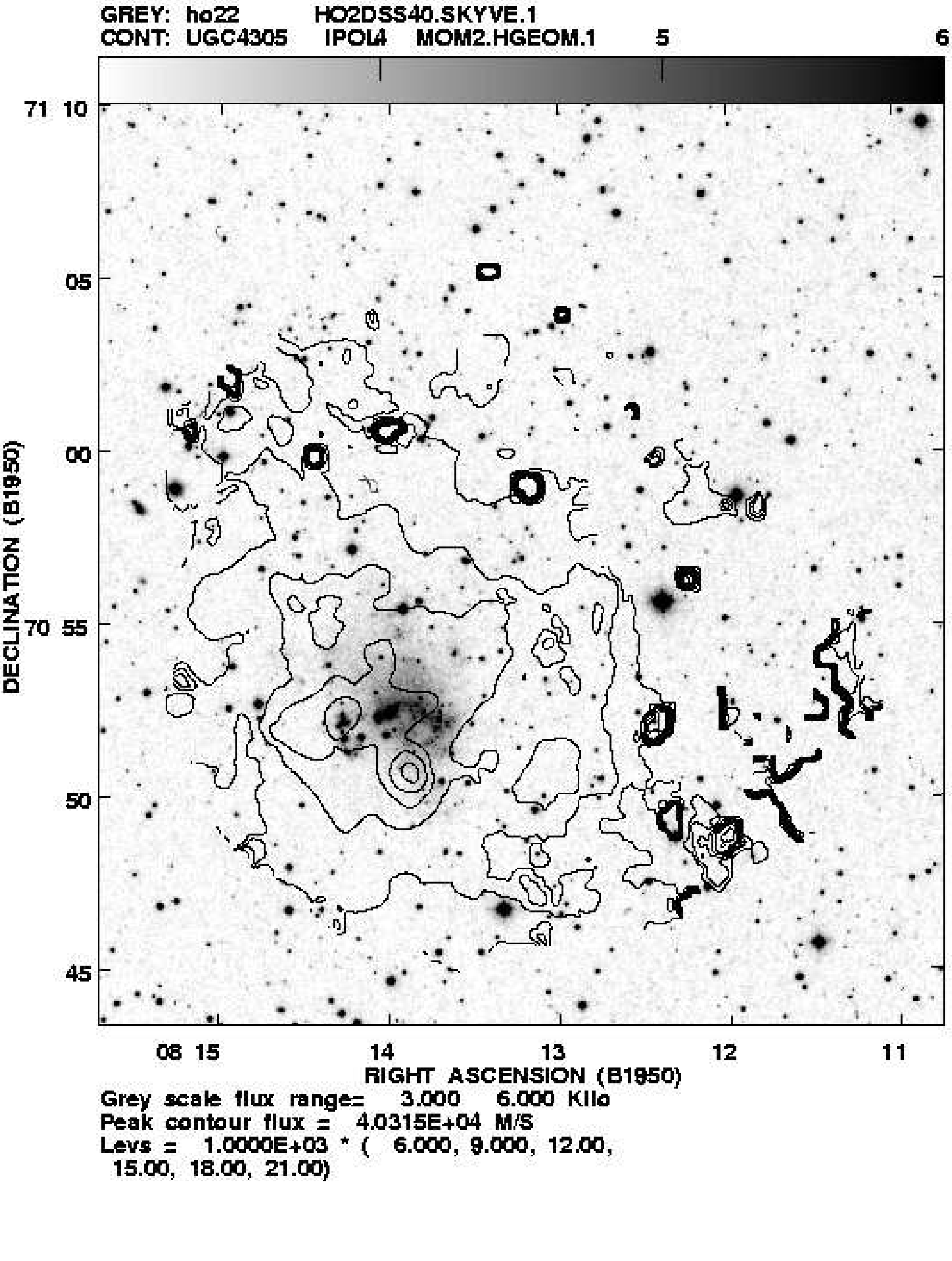
GREY: ho22 HO2DSS40.SKYVE.1
CONT: UGC4305 IPOL4 MOM2.HGEOM.1
5
6
71 10
05
00
70 55
50
45
DECLINATION (B1950)
08 15
14
13
12
11
RIGHT ASCENSION (B1950)
Grey scale flux range= 3.000 6.000 Kilo
Peak contour flux = 4.0315E+04 M/S
Levs = 1.0000E+03 * (6.000, 9.000, 12.00,
15.00, 18.00, 21.00)